AIP | The Journal of Chemical Physics

Quantum dynamics of hydrogen atoms on graphene. I. System-bath modeling

Matteo Bonfanti, Bret Jackson, Keith H. Hughes, Irene Burghardt, and Rocco Martinazzo

Citation: The Journal of Chemical Physics **143**, 124703 (2015); doi: 10.1063/1.4931116
View online: http://dx.doi.org/10.1063/1.4931116
View Table of Contents: http://scitation.aip.org/content/aip/journal/jcp/143/12?ver=pdfcov
Published by the AIP Publishing

Quantum dynamics of hydrogen atoms on graphene. I. System-bath modeling

Matteo Bonfanti,[1,a)] Bret Jackson,[2] Keith H. Hughes,[3] Irene Burghardt,[4] and Rocco Martinazzo[1,5,b)]
[1]*Dipartimento di Chimica, Università degli Studi di Milano, v. Golgi 19, 20133 Milano, Italy*
[2]*Department of Chemistry, University of Massachusetts, Amherst, Massachusetts 01003, USA*
[3]*School of Chemistry, Bangor University, Bangor, Gwynedd LL57 2UW, United Kingdom*
[4]*Institute of Physical and Theoretical Chemistry, Goethe University Frankfurt, Max-von-Laue-Str. 7, 60438 Frankfurt/Main, Germany*
[5]*Istituto di Scienze e Tecnologie Molecolari, Consiglio Nazionale delle Richerche, v. Golgi 19, 20133 Milano, Italy*

(Received 22 July 2015; accepted 4 September 2015; published online 23 September 2015)

An accurate system-bath model to investigate the quantum dynamics of hydrogen atoms chemisorbed on graphene is presented. The system comprises a hydrogen atom and the carbon atom from graphene that forms the covalent bond, and it is described by a previously developed 4D potential energy surface based on density functional theory *ab initio* data. The bath describes the rest of the carbon lattice and is obtained from an empirical force field through inversion of a classical equilibrium correlation function describing the hydrogen motion. By construction, model building easily accommodates improvements coming from the use of higher level electronic structure theory for the system. Further, it is well suited to a determination of the system-environment coupling by means of *ab initio* molecular dynamics. This paper details the system-bath modeling and shows its application to the quantum dynamics of vibrational relaxation of a chemisorbed hydrogen atom, which is here investigated at $T = 0$ K with the help of the multi-configuration time-dependent Hartree method. Paper II deals with the sticking dynamics. © *2015 AIP Publishing LLC.* [http://dx.doi.org/10.1063/1.4931116]

I. INTRODUCTION

In the last decade, hydrogen sticking on graphitic/graphenic surfaces has been one of the most studied gas-surface scattering problems. Apart from being a challenging model system for which a variety of experimental results is available, the interest in the hydrogen sticking on graphene has been mainly triggered by focus issues in two different research fields. First, since the 2010 Nobel Prize for graphene discovery, chemical modification of graphene has been considered a possible route for the development of carbon based materials which might couple the extraordinary electronic, mechanical, and thermal properties of graphene with the presence of a band gap.[1,2] Second, it has been long established that molecular hydrogen formation in the interstellar medium (ISM) proceeds via surface chemistry at the carbonaceous, graphitic-like surfaces of dust particles. Thus, hydrogen adsorption on graphite is considered a key step for the ISM chemistry and its quantification is fundamental for the development of astrophysical models of star evolution.[3–5]

The energetics of hydrogen adsorption has been extensively studied, mostly at the Density Functional Theory (DFT) level with the periodic supercell approach[6–10] and more lately with some accurate wavefunction calculations on cluster models.[11–14] Many different aspects of hydrogen adsorption have been addressed, including adsorption and diffusion in the shallow physisorption well,[11] single and multiple adsorption in the chemisorption well,[9,15–17] carbon vacancy hydrogenation,[18] and binding to edges.[13,19] All these possibilities determine a vast variety of cases which can be well interpreted and rationalized in terms of electronic and structural effects.

While the energetics of hydrogen adsorption has been well understood and the dynamics of sticking and diffusing hydrogen in the ~40 meV physisorption state have been accurately described,[11,20–22] there are still unsettled issues concerning chemisorption that need further investigations. First, the accurate value of the barrier height is still not clear. On one hand, most DFT periodic calculations in the Generalized Gradient Approximation (GGA) give a barrier of ~0.2 eV-a value which is considerably reduced when van der Waals corrected functionals are employed.[23] On the other hand, accurate wavefunctions calculations on cluster models by Wang *et al.*[14] suggest that GGA functionals overestimate the binding energy, hence underestimate the barrier (by more than 0.2 eV, see Ref. 14). Second, at any coverage but the lowest (say, above 1%), hydrogen has shown a tendency for clustering,[15,24,25] as a consequence of the extended aromatic nature of graphene/graphite and accounting for this requires a number of different adsorption situations with very different reaction barriers.[9,26] Finally, despite the apparent simplicity of the system, building a dynamical model which is suited to study the process in the low collision energy regime remains a challenging problem. Many models have been proposed in the past, highlighting that many different effects need to be simultaneously accounted for to reach a quantitative

a)Electronic mail: matteo.bonfanti@unimi.it
b)Electronic mail: rocco.martinazzo@unimi.it

description of the process:[23,26–32] (i) due to the fast substrate relaxation induced by the sp^2–sp^3 conversion, forces on the binding carbon atom are large and the motion of the latter is strongly coupled to the hydrogen coordinate;[27] (ii) a large fraction of the reaction takes place at the non-collinear geometries, since steering of the projectile is operative;[28] (iii) energy relaxation to graphene phonons is a relatively fast process and large amounts of energy need to be transferred such that saturation effects are likely when truncating the phonon basis;[26,32] and (iv) quantum effects have large consequences on the sticking probability, particularly at the low incident energies of interest for the chemistry of the ISM where tunneling dominates.[23,28,30,31]

In the present work, we devise a model for hydrogen chemisorption that takes into account all the requirements listed above and use it in a fully quantum study of the sticking dynamics. The model consists of an accurate description of the hydrogen atom and its bonding carbon atom, which are coupled to the graphene substrate described by a phonon bath. Both system and phonon bath are treated with numerically exact, high dimensional quantum dynamical methods.

The model presented below is based on the potential energy surface (PES) of the -CH moiety developed a while ago by one of the present authors and his collaborators.[20,28] This "system potential" is given as an analytical functional form fitted to the results of periodic, plane-wave DFT calculations,[28] which used a simple, semi-local approximation to the exact exchange-correlation functional (the PW91 GGA functional). As for the coupling of the CH bond to the rest of the graphene surface, the model relies on *dynamical* information which is here retrieved from equilibrium molecular dynamics (MD) simulations of the CH system connected to an accurate force field of the lattice[33] via a Surface Oscillator (SO) model-type coupling.[20] The overall modeling though has been designed to be "modular," and work is already in progress to improve both the CH description and the system-environment coupling, exploiting the progress in density functional theory and the increase of computational resources that have occurred since the work of Refs. 20 and 28. Among these developments, noteworthy is the formulation of accurate vdW-DFT functionals which overcome some of the limitations of the semi-local functionals,[34,35] namely, the inability to describe non-local dispersion forces which have been shown recently to affect both the physisorption well and the sticking barrier in the present problem.[23] Furthermore, the increasing feasibility of direct, *ab initio* molecular dynamics approaches allows one to bypass the need of developing lattice potentials and modeling the system-environment coupling when describing energy transfer to the surface.

In the present paper, henceforth denoted Paper I, we derive the model, check its consistency, and use it to study the relaxation of a vibrationally excited adsorbed hydrogen. In the following paper,[57] henceforth denoted Paper II, we extend the approach to the quantum dynamical, dissipative scattering setting needed to investigate sticking of a hydrogen atom to the graphene surface.

This paper is organized as follows. In Section II, we present the methodology we developed for the construction of our model Hamiltonian. In Section III, we give a brief account of the properties of the H-graphene potential energy surface. In Section IV, we briefly describe the methodology employed for performing the classical and quantum dynamical simulations, and in Section V, we present our main results. Finally, Section VI summarizes and concludes.

II. THEORY

Fully atomistic potential models, irrespective of their origin and of their quality, are not suited for high dimensional quantum dynamical simulations. Strong coupling within sparse sets of degrees of freedom (DOFs, most often irrelevant for the problem of interest) prevents the use of any general truncation scheme that is crucial for applying numerical methods. In order to make progress in investigating the sticking dynamics of interest, we rely on the following assumptions: (i) the energy exchange that occurs between the system and the lattice for near equilibrium configurations is representative of energy dissipation; (ii) relaxation proceeds through sequential energy transfer from the hydrogen atom to the carbon atom, which is in turn the only one directly coupled to the rest of the lattice through its height coordinate z_C above the surface; and (iii) a mapping holds, at least approximately, which relates the classical Hamiltonian dynamics of the interesting C and H atoms to a generalized Langevin equation (GLE) description. In (iii), it is inferred that if the system is a single degree of freedom s, generally referred to as the "Brownian particle," its dynamics can be described by the GLE

$$m\ddot{s}(t) + m\int_{-\infty}^{+\infty} \gamma(t-\tau)\dot{s}(\tau)d\tau + V'(s(t)) = \xi(t), \quad (1)$$

where $\gamma(t)$ is a memory kernel obeying causality ($\gamma(t) = 0$ for $t < 0$) and $\xi(t)$ a Gaussian stochastic process related to $\gamma(t)$ by a fluctuation-dissipation theorem of the second kind, $\langle \xi(t)\xi(0)\rangle = \gamma(|t|)k_BT/m$. Here, and in the following, $\langle ..\rangle$ denotes an average over the canonical equilibrium, T is the temperature, and k_B the Boltzmann constant. The advantage of using (iii) is the equivalence of the above GLE with the dynamics generated by the Independent Oscillator (IO) (also known as Caldeira-Leggett) Hamiltonian[36]

$$H^{IO} = \frac{p_s^2}{2m} + V(s) + \sum_{k=1}^{F}\left[\frac{p_k^2}{2} + \frac{\omega_k^2}{2}\left(q_k - \frac{c_k}{\omega_k^2}s\right)^2\right]. \quad (2)$$

For a finite number of oscillators F, a strict equivalence between Eqs. (1) and (2) only holds for times less than the Poincaré recurrence time t_{rec}, and provided the bath oscillator frequencies ω_k and coupling coefficients c_k sample the so-called spectral density (SD) of the environmental coupling.[36] The latter is defined as $J(\omega) = m\omega\Re\tilde{\gamma}(\omega)$, where $\tilde{\gamma}(\omega) = \int_{-\infty}^{+\infty}\gamma(t)e^{i\omega t}dt$ is the frequency-dependent memory kernel. The SD fully determines $\tilde{\gamma}(\omega)$, hence the GLE, by virtue of the celebrated Kramers-Kronig relation, and thus contains all the necessary information about the coupling of the system to the environment. For an evenly spaced set of frequencies $\omega_k = k\Delta\omega$, the couplings read as $c_k = \sqrt{2\omega_k\Delta\omega J(\omega_k)/\pi}$ and $t_{rec} = 2\pi/\Delta\omega$. The advantage of an IO Hamiltonian description is of course that it provides a much simpler (but equivalent) model of the original atomistic Hamiltonian, whose quantized

version can be tackled with numerically exact wavepacket techniques up to several tens of DOFs.

Clearly, in studying the sticking of H atoms in the chemisorption regime, both the H and the binding C atom need to be included in the "Brownian" particle. Hence, assumption (ii) described above, relating to a sequential energy transfer from hydrogen to carbon, and from carbon to the lattice, implies that the GLE remains effectively one-dimensional (as opposed to a more general *multidimensional* GLE) and that the relevant (scalar) spectral density describes the coupling of the binding C atom with the rest of the surface. In other words, the final, working IO model takes the form[37]

$$H = \frac{\mathbf{p}_H^2}{2m_H} + \frac{p_C^2}{2m_C} + V_s(\mathbf{x}_H, z_C) + \sum_{k=1}^{F}\left[\frac{p_k^2}{2} + \frac{\omega_k^2}{2}\left(q_k - \frac{c_k}{\omega_k^2}(z_C - z_C^{eq})\right)^2\right], \quad (3)$$

where $\mathbf{x}_H$ is the position of the H atom, z_C the height of the binding C atom above the surface, $\mathbf{p}_H$ and p_C the corresponding momenta, and $V_s(\mathbf{x}_H, z_C)$ an appropriate 4D system potential (see Fig. 1 for the definition of the system coordinates). The frequencies ω_k and couplings c_k of the IO bath sample a spectral density $J_C(\omega)$ that describes the coupling of the C atom to the rest of the lattice. Constructing the latter represents one of the main goals of our system-bath modeling that, according to assumption (i), can be accomplished with the help of classical (canonical) molecular dynamics simulations of the *equilibrium* state of the H-graphene system. In Section II A, it is shown how assumption (i) above (along with (ii)) can be exploited to obtain $J_C(\omega)$ from the equilibrium dynamics of the *hydrogen* atom above the surface (z_H); Sec. II B gives some details about the choice of the system potential.

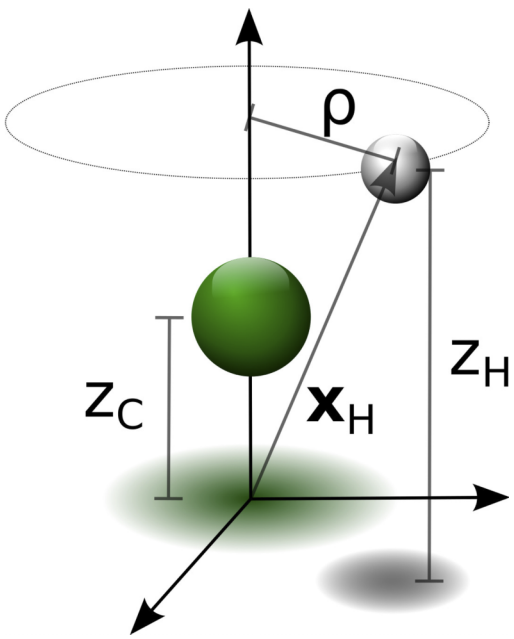

FIG. 1. Schematic illustration of the coordinates adopted for the description of the CH system.

A. Spectral density

For small oscillations around the equilibrium position z_H^{eq}, the height of the hydrogen atom undergoes Harmonic Brownian motion

$$\ddot{z}_H(t) + \int_{-\infty}^{+\infty} \gamma_H(t-\tau)\dot{z}_H(\tau)d\tau + \omega_0^2 z_H(t) = \xi_H(t)/m_H$$

(where ω_0 is its frequency and γ_H,ξ_H characterize its environment), and the equilibrium correlation function of its displacement $C_H(t) = \langle \delta z_H(t)\delta z_H(0)\rangle = \langle (z_H(t) - z_H^{eq})(z_H(0) - z_H^{eq})\rangle$ is related to the memory kernel through[38]

$$\frac{1}{2}\omega\tilde{C}_H(\omega) = \frac{k_B T}{m_H}\Im\left(\frac{1}{\omega_0^2 - \omega^2 - i\omega\tilde{\gamma}_H(\omega)}\right). \quad (4)$$

Here, $\tilde{C}_H(\omega) = \int e^{i\omega t}C_H(t)dt$ is the frequency dependent correlation function.[39] As shown in Ref. 40, this equation can be "inverted" to give the spectral density $J_H(\omega) = m_H\omega\Re\tilde{\gamma}_H(\omega)$ in terms of $\tilde{C}_H(\omega)$,

$$J_H(\omega) = \frac{k_B T}{2}\frac{\omega\tilde{C}_H(\omega)}{|\Gamma^+(\omega)|^2}, \quad (5)$$

where $\Gamma(z)$ is the "Cauchy transform" of the function $\tilde{C}_H(\omega)\omega/2$,

$$\Gamma(z) = \frac{1}{\pi}\int_{-\infty}^{+\infty}\frac{\omega\tilde{C}_H(\omega)/2}{\omega - z}d\omega$$

and $\Gamma^+(\omega) = \lim_{\epsilon\to 0^+}\Gamma(\omega + i\epsilon)$ is its limit on the real axis from the upper half plane. (As was shown in Ref. 40, one can equivalently define $\Gamma(z) = iz\hat{C}_H(z) + C_H(0)$, where $\hat{C}_H(z) = \int_0^\infty e^{izt}C_H(t)dt$ ($\Im z > 0$) is the Fourier-Laplace transform of the retarded correlation function.)

The spectral density $J_H(\omega)$ describes the coupling of the hydrogen atom to its environment which, according to our assumption (ii), reduces to the height z_C of the binding C atom that *in turn* couples to the rest of the surface. Hence, the coordinate z_C is, to within a mass factor, the first effective mode in the general effective-mode transformation that brings the environment felt by the hydrogen atom into a linear chain form.[41–44] Using the results of Ref. 43, the required spectral density follows from

$$J_C(\omega) = \frac{D_C^2 J_H(\omega)}{|W_H^+(\omega)|^2}, \quad (6)$$

where

$$D_C^2 = \frac{2m_C}{\pi}\int_0^\infty J_H(\omega)\omega d\omega$$

is the relevant effective mode coupling and $W_H(z)$ is the Cauchy transform of $J_H(\omega)$,

$$W_H(z) = \frac{1}{\pi}\int_{-\infty}^{+\infty}\frac{J_H(\omega)}{\omega - z}d\omega.$$

Eqs. (5) and (6) are the working equations, giving explicitly the SD felt by the C atom in terms of $C_H(t)$. Together with the system potential to be specified below, Eqs. (5) and (6) allow us to completely define the Hamiltonian model of Eq. (3). They require as input some information about the equilibrium dynamics of the adsorbed H atom above the surface, which might come from spectroscopic data or, more commonly, from simple, unconstrained canonical molecular dynamics. To this end,

a "source" for such equilibrium dynamics has to be defined. In this work, we used classical dynamics simulations based on the successful atomistic model developed some years ago by Kerwin and Jackson[26] (see Section III), since this choice allows us to compare our results with the available literature data. We stress though that Eqs. (5) and (6) make use of only dynamical information and are well suited to an *ab initio* molecular dynamics approach, thereby bypassing the need of the time-consuming steps that are required for building an atomistic model.

B. System potential

Once the coupling of the C atom with its environment has been defined with the aid of the corresponding spectral density $J_C(\omega)$, the working Hamiltonian model of Eq. (3) is completely specified by defining the system potential $V_s(\mathbf{x}_H, z_C)$ that describes the interaction of the H atom with the binding carbon. From the form of Eq. (3), provided that condition (iii) holds, the system potential should describe the interactions within the system in the partial equilibrium state where the bath coordinates minimize the total potential for each value of the system coordinates $(\mathbf{x}_H, z_C)$. Accordingly, we define the system potential as

$$V_s(\mathbf{x}_H, z_C) = \underset{\{\mathbf{Q}\}}{\text{Min}}\, V_{at}(\mathbf{x}_H, z_C, \mathbf{Q}), \tag{7}$$

where V_{at} is the atomistic model of the H-graphene system mentioned above,[26] which is based on an analytic fit to *first-principles* data[28] and on an empirical lattice model for graphene.[33] This potential is a function of a number of lattice coordinates $\{Q_1, Q_2, \ldots, Q_N\} = \mathbf{Q}$ and is described in some detail below since it is also our source model for the spectral density of the binding carbon atom. Here, we note that the system potential V_s as defined by the above equation differs only marginally from the original CH potential of Ref. 26 but its introduction is unavoidable if a strict comparison has to be made between the system-bath dynamics and the one resulting from the lattice model.

III. THE "SOURCE" MODEL

As mentioned above, an atomistic interaction potential[26] was used to generate the necessary dynamical information on the system. This potential was obtained by connecting an accurate C–H system potential V_{CH} to an empirical graphene force field, via a surface oscillator model-type coupling.[45] The analytic form of the C–H potential is described in detail in Ref. 28. It is given as a function of three coordinates, $V_{CH}^{3D} = V_{CH}^{3D}(z_H, z_C, \rho)$, two for the hydrogen atom and one for the nearest carbon atom, namely, the height of the two above the surface (z_H and z_C, respectively) and the projection of the C–H bond length onto the surface (ρ). In our simulations, we preferred to re-express the potential as a function of the in-plane Cartesian coordinates of the hydrogen atom, namely, with $\mathbf{x}_H^{\parallel} \equiv (x_H, y_H)$ and the C atom at the origin, we set $V_{CH}(\mathbf{x}_H^{\parallel}, z_H, z_C) = V_{CH}^{3D}(z_H, z_C, \|\mathbf{x}_H^{\parallel}\|)$. We thus adopted a redundant set of variables that does not exploit the cylindrical invariance of the original PES that was well supported by the *ab initio* data.[28] This choice results in a simpler representation of the kinetic energy operator and easily accommodates any improvements of the system potential that may result from relaxing the assumption of a rotationally invariant interaction.[28]

The graphene phonon potential is a force field for a cluster of a total of 121 carbon atoms with in-plane coordinates (X_α, Y_α) fixed and arranged in a honeycomb lattice. This part of the PES is thus a function of 121 displacement of the atoms normal to the surface z_α (including the C atom that the hydrogen binds to, which in this context may be referred to as C_0), and describes graphene transverse phonons only, i.e., the transverse acoustical (flexural) mode ZA and the transverse optical mode (ZO).[46] This approximation seems to be reasonable for the sticking problem of interest, and although not essential for the success of the model, motivation for the approximation was the simpler coding of the lattice model that it allows for, when compared to the original, accurate but rather complicated force field developed by Aizawa *et al.*[33]

The C–H system and the graphene lattice are coupled to each other through a SO model-type coupling, namely,

$$V_{at}(\boldsymbol{x}_H, z_C, \mathbf{Q}) = V_{CH}(\mathbf{x}_H^{\parallel}, z_H - Q_0, z_C - Q_0) + V_l(z_C, z_1, \ldots, z_N) - \frac{1}{2}k_C(z_C - Q_0)^2,$$

where $Q_k \equiv z_k$ are the heights of the carbon atoms other than C_0, Q_0 is the average height of the three carbon atoms closest to the adsorption site, $Q_0 = (z_1 + z_2 + z_3)/3$, V_l is the Aizawa *et al.*[33] lattice potential for transverse motion, and the rightmost term avoids double counting (k_C being the force constant for the puckering of C_0 alone, as obtained from the lattice model).[26]

In agreement with the well established picture of hydrogen chemisorption on graphene, the adopted potential predicts that in the minimum energy structure the surface "puckers" to allow the $sp^2 \rightarrow sp^3$ re-hybridization necessary for the carbon atom to bind the hydrogen atom. This surface reconstruction brings the carbon atom 0.426 Å out of the plane defined by the three nearest neighbor carbon atoms and allows the H atom to form a relatively strong (0.767 eV) σ bond with the puckered C atom which is 1.11 Å long. To reach this stable configuration from the gas-phase along the minimum energy path, the hydrogen atom has to overcome an energy barrier 0.235 eV high, which is found at $z_H = 1.97$ Å and $z_C = 0.110$ Å. The potential further features a shallow physisorption well (~9 meV deep) when the hydrogen atom is far (~3.0 Å) from the surface, which is though far from the accepted value of ~40 meV, as obtained from the analysis of selective adsorption resonances in scattering experiments[47] and confirmed by accurate wavefunction-based calculations.[11]

We computed the phonon density of states (DOS) of the model cluster by performing a normal mode analysis, in which the Hessian matrix was obtained with first order finite differences of the analytic first derivatives of the potential. Fig. 2 shows both the DOS computed when the hydrogen atom is far from the surface (where the potential reduces to the force field of the lattice) and the DOS in the stable adsorption geometry. When the hydrogen atom is far from the surface, we see that

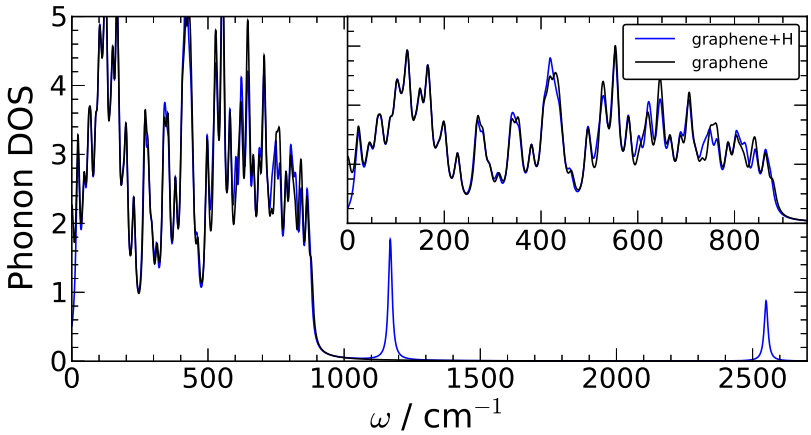

FIG. 2. Total density of phonon states obtained from the potential of Ref. 26 in two limiting cases. Black line for the case where the hydrogen atom is far from the flat surface. Blue line for H adsorbed on the puckered surface. The inset is a close-up of the spectral region of graphene, between 0.0 and 900.0 cm^{-1}. Eigenmodes have been Gaussian broadened by 8 cm^{-1} to mimic a continuous density of state.

the highest frequency peak in the spectrum occurs at 874 cm^{-1}, consistent with a model containing only transverse optical and acoustic phonon branches.[33] Hydrogen adsorption introduces two new modes at frequencies well above the graphene region: one stretching mode at 2549 cm^{-1} and a twofold degenerate bending at 1169 cm^{-1}. Furthermore, some of the carbon cluster frequencies are shifted, as a consequence of the puckering of the graphene sheet and of the strong coupling of a carbon atom with the adsorbate.

In light of this separation between the C–H system and the graphene phonon bath, we further looked at the normal modes of the 4D system potential only, which were obtained by fixing all the lattice coordinates in the equilibrium geometry, except the one involved in the CH bond. The resulting four normal modes are

- a doubly degenerate bending at 1169.48 cm^{-1} , which only involves displacements of ρ and is thus completely uncoupled from the z coordinates (at the harmonic level);
- a 2549.36 cm^{-1} C–H stretching mode;
- a 466.50 cm^{-1} "surface" stretching mode, which approximately corresponds to block oscillations of the C–H unit above the surface plane.

The lack of coupling between ρ and the other z coordinates is a direct consequence of the cylindrical symmetry of the potential itself,[28] which demands it be quadratic everywhere in ρ at quasi-collinear configurations, $V^{3D}_{CH}(z_H, z_C, \rho) \approx \rho^2 \kappa(z_H, z_C)$, i.e., in the neighborhoods of the minimum structure ($\rho = 0$). Hence, the lateral displacement does not mix with either z_C or z_H in the equilibrium configuration ($\partial^2 V^{3D}_{CH}/\partial\rho\partial z|_{\rho=0} = 0$ for $z = z_H$ or z_C).

It should be noted that both the C–H bending and the stretching frequencies hardly change from their full DOS values when constraining the lattice carbon atoms in plane. These vibrations are well above the graphene cut-off ("Debye") frequency and are thus dynamically decoupled from the graphene bath. In contrast, the surface stretching mode, which is very similar to a carbon atom normal displacement, is well within the surface phonon band and strongly coupled to the lattice.

Overall, our findings are in excellent agreement with the *first principles* results of Sakong and Kratzer,[48] who used a larger (five dimensional) dynamical matrix and found the C–H stretching at 2552 cm^{-1} and two bending modes at 1175 and 1110 cm^{-1}. Of course, differently from Fig. 2, the phonon DOS of Ref. 48 extends up to 1583 cm^{-1} because of the inclusion of the higher frequency longitudinal and shear optical branches.[33]

IV. TECHNICALITIES

A. Classical molecular dynamics

Classical, equilibrium MD simulations were performed with the potential energy surface described above. These simulations were then used to compute the autocorrelation function of the displacement of the hydrogen atom from its equilibrium structure and the spectral functions according to Eqs. (5) and (6). Thermal averages were computed over a set of trajectories with initial conditions sampling the canonical distribution, after a preliminary equilibration stage accomplished via standard Langevin dynamics of each carbon atom of the lattice (i.e., with white noise). After the equilibration stage, Langevin dynamics was turned off everywhere except at the edges of the carbon cluster, in order to mimic an infinite carbon slab. During this second part of the dynamics, the dynamical variable z_H was sampled.

Time propagation was performed with a symplectic propagator for Langevin dynamics[49] that reduces to the velocity-Verlet propagator when the damping is turned off ($\gamma \to 0$). Table I summarizes the main parameters of the MD simulations. The relaxation rate at the cluster edges was set to $\gamma^{-1} = 100$ fs and was chosen after carefully checking that it guarantees a reasonable broadening of the peaks without

TABLE I. Integration parameters of the MD simulations performed with the "source" atomistic model.

No. of trajectories	1000
Equilibration Δt	0.02 fs
Equilibration $\tau_{\text{relax}} = \gamma^{-1}$	5.0 fs
Equilibration time	2.0 ps
Propagation Δt	0.01 fs
Relax at the edges τ_{edges}	100.0 fs
Propagation time	10.0 ps
Time step of trajectory sampling	0.5 fs

strongly affecting the fine structure of the correlation functions; furthermore, a $\gamma^{-1} = 100$ fs relaxation time is comparable to the one expected for the coupling of the carbon cluster with the rest of the graphene sheet.

The accumulated realizations $\delta z_H^i(t) = z_H^i(t) - z_H^{eq}$ were then Fourier-transformed and used to compute the frequency-dependent correlation function $\tilde{C}(\omega)$ with the help of the Wiener-Khinchin theorem,[38]

$$X_{t_f}^i(\omega) = \int_0^{t_f} \delta \tilde{z}_H^i(t) e^{i\omega t} dt, \quad \tilde{C}(\omega) = \frac{1}{t_f} |\mathbf{X}_{t_f}(\omega)|_{av}^2$$

(where av stands for the average over the realizations of the random variable $\mathbf{X}_{t_f}$) and could, in principle, be directly used to obtain the hydrogen atom spectral density $J_H(\omega)$ and the carbon atom spectral density $J_C(\omega)$ as outlined in Section II. In practice though, we first had to smoothen the peaks of the spectra, by applying a Gaussian damping in the time-domain with a 1.0 ps relaxation time and then to filter out undesirable high-frequency components. Indeed, while the total propagation time of the trajectories gives a reasonably narrow frequency spacing of 3.34 cm^{-1}, the adopted time step gives rise to a frequency cutoff larger than 60 000 cm^{-1}, thereby including a wide frequency region where the use of the Cauchy transforms becomes numerically awkward because of the vanishing small spectral weights. The adopted lower cutoff of $\omega_C = 4000$ cm^{-1} is a reasonable "unbiased" choice, yet larger than the Debye cut-off frequency ω_D of the graphene sheet ($\omega_D = 874$ cm^{-1} in our model, see Fig. 2). As a result, the spectral densities still contain some undesired high frequency features recently discussed in Ref. 40 and, in particular, a growing base line that is due to the slow decay of $\tilde{C}(\omega)$ above ω_D. To remedy this numerical problem, we applied a low frequency filter to damp out the high frequency contributions, namely, we defined the working frequency-dependent correlation function $\tilde{C}_H(\omega)$ as

$$\tilde{C}_H(\omega) = \tilde{C}(\omega)\,[1 + f(\omega)]\,, \tag{8}$$

where[50]

$$f(\omega) = \left[\left(\frac{\omega_0}{\omega}\right)^N - 1\right] \times \exp\left(\frac{\omega_0^N}{\omega_0^N - \omega^N}\right) \Theta(\omega - \omega_0)$$

($\Theta(x) = 1$ for $x \geq 0$ and zero otherwise), $\omega_0 = 2541.0$ cm^{-1}, and $N = 12$. The filtering function tends to -1 at large ω and goes smoothly to zero for $\omega \to \omega_0^+$.

B. Quantum dynamics

High dimensional, quantum dynamical calculations were carried out using the multi-configuration time-dependent Hartree (MCTDH) method (Heidelberg package[51–54]), for the system and a discrete sampling of the bath modes. The system-bath coupling strengths c_k were obtained from the spectral density $J_C(\omega)$ describing the interaction of the carbon atom C_0 with the rest of the lattice, $c_k = \sqrt{2\omega_k \Delta\omega J_C(\omega_k)/\pi}$, with $\omega_k = k\Delta\omega$ and for $k = 1, \ldots, F$, with an appropriate number F of oscillators (see below). In this paper, vibrational relaxation is used for illustrative purposes, while Paper II is devoted to simulations of the sticking process.

The 4D system potential $V_s(\boldsymbol{x}_H, z_C)$ as defined in Eq. (7) was used as a reference to generate approximate vibrational eigenstates of the system, by using an exact (Lanczos) diagonalization scheme. These functions were then used to generate several product initial states with the ground-state wavefunction of the uncoupled bath, which were later propagated in time under the action of the full IO Hamiltonian. For the primitive Discrete Variable Representation (DVR) grid, we used a Hermite basis set for all the degrees of freedom—10 points for z_H, 30 for z_C, 5 for x_H, and y_H and 6 for each of the x_k's—with appropriate masses and harmonic frequencies. The adopted mode-combination scheme and the number of single particle functions (spf's) are summarized in Table II and were carefully checked to give well converged results. Note that the system was described with a single mode while the bath oscillators were grouped in modes of five degrees of freedom.

Because of the unfavorable scaling of quantum dynamics with the number of degrees of freedom, the bath sizes were limited to 50 or 75 oscillators. To achieve a good sampling of the spectral density, the equally spaced bath frequencies were focused in the spectral region most relevant for the various relaxation processes considered. Thus, in the case of the relaxation of the surface stretching normal mode, we used a 0-900 cm^{-1} bath, whereas when investigating relaxation of the C–H stretching mode, we focused on the range 2100-2900 cm^{-1}. These spectral regions were extended for investigating bending relaxation and when excitation involved more than one mode, where both the low (0-900 cm^{-1}) and the high (2100-2900 cm^{-1}) frequency regions were sampled. These reduced sampling schemes were carefully checked against simulations using a uniform sampling of the SD in the 0-4000 cm^{-1} range (not shown). Apart from obvious differences due to the shorter recurrence time and the coarser sampling of the latter, a good agreement was found between the two sets of calculations.

TABLE II. Mode-combination scheme and number of single particle functions used in the MCTDH quantum dynamical simulations described in the main text.

Bath size	F = 50	F = 75	F = 75
Frequency range / cm^{-1}	[0, 900]	[2100, 2900]	[0, 900] + [2100, 2900]
System	8	8	7
$q_1 \ldots q_5$	3	2	2
$q_6 \ldots q_{10}$	3	2	3
$q_{11} \ldots q_{15}$	3	3	3
$q_{16} \ldots q_{20}$	4	3	3
$q_{21} \ldots q_{25}$	4	3	3
$q_{26} \ldots q_{30}$	4	3	3
$q_{31} \ldots q_{35}$	4	3	3
$q_{36} \ldots q_{40}$	4	3	3
$q_{41} \ldots q_{45}$	4	3	2
$q_{46} \ldots q_{50}$	3	2	2
$q_{51} \ldots q_{55}$		2	2
$q_{56} \ldots q_{60}$		2	4
$q_{61} \ldots q_{65}$		2	2
$q_{66} \ldots q_{70}$		2	2
$q_{71} \ldots q_{75}$		2	2

V. RESULTS AND DISCUSSION

A. Spectral densities

A number of MD simulations for several temperatures in the range 5-300 K were performed, and for each temperature 1000 trajectories were run, with dissipation at the cluster edges, according to the parameters given in Table I. This number is sufficient to obtain well converged results and, importantly, is well within the limit of an *ab initio* molecular dynamics approach. Fig. 3 shows the results of these calculations, namely, the frequency-dependent correlation function of the H atom displacement $\tilde{C}_H(\omega)$, and the spectral densities $J_H(\omega)$ and $J_C(\omega)$ obtained upon application of Eqs. (5) and (6). As is evident from panel (a) of Fig. 3, two main structures appear in $\tilde{C}_H(\omega)$: a broad band at low frequencies, in the 0-900 cm^{-1} region, and a narrow peak at approximately 2500 cm^{-1}, which is consistent with phonon spectrum and the normal mode analysis of the system given in Section III (for the purpose of a comparison notice that in Fig. 3 above $\tilde{C}(\omega)$ is given on a logarithmic scale). The low frequency region is associated with the surface stretching mode, which is strongly coupled to and mixed with the lattice modes; this is manifested in a rather broad band that has the width of the DOS of the cluster. In contrast, the peak of the C–H stretching mode stands out from a marginal background, in line with the lower frequency cutoff of the bath. As discussed in Ref. 40, in such a situation where the system frequency exceeds the Debye frequency of the environment, only a δ-peak should ideally appear in a bilinear coupling model. In realistic situations, some broadening always occurs, for at least three main reasons: (i) the system anharmonicities (see below), (ii) the failure of the bilinear coupling assumption, and (iii) the dissipative-like trajectory propagation conditions. The first arises because anharmonic effects in the system potential cannot be handled with the approach outlined in Section II, and need to be known in advance. They are readily recognized by their characteristic temperature-dependent behavior, which makes them more pronounced when the vibrator explores all regions of the potential more extensively. Similarly for the effects of the failure of the bilinear-coupling model, they are expected to become more evident when increasing the temperatures. They are more subtle than the system anharmonicities but, differently from them, are representative of *true* system-environment interactions and can be likely mapped into an "extended" bilinear model, where bath modes appear with frequencies *larger* than the Debye frequency of the true environment. Finally, the third cause of broadening is due to the algorithmic nature of the molecular dynamics approach (e.g., the presence of thermostats or the use of damping functions) and is simply impossible to eliminate in any real numerical application.

As is evident from Fig. 3 (panel (a)), the low frequency region is extremely stable with temperature, thereby suggesting that this spectral region provides a sound and coherent representation of a real coupling between the hydrogen atom oscillations and the bath of lattice phonons. On the other hand, the high frequency region is strongly temperature-dependent and presents a peak which progressively broadens when increasing the temperature. As will be shown below, this effect is mainly due to the anharmonicity of the C–H system and thus should *not* be attributed to the stochastic properties of the environment. This is not a real problem for the IO model of Eq. (3), since the latter uses a full anharmonic potential for the C–H vibrator and thus includes these effects by construction.

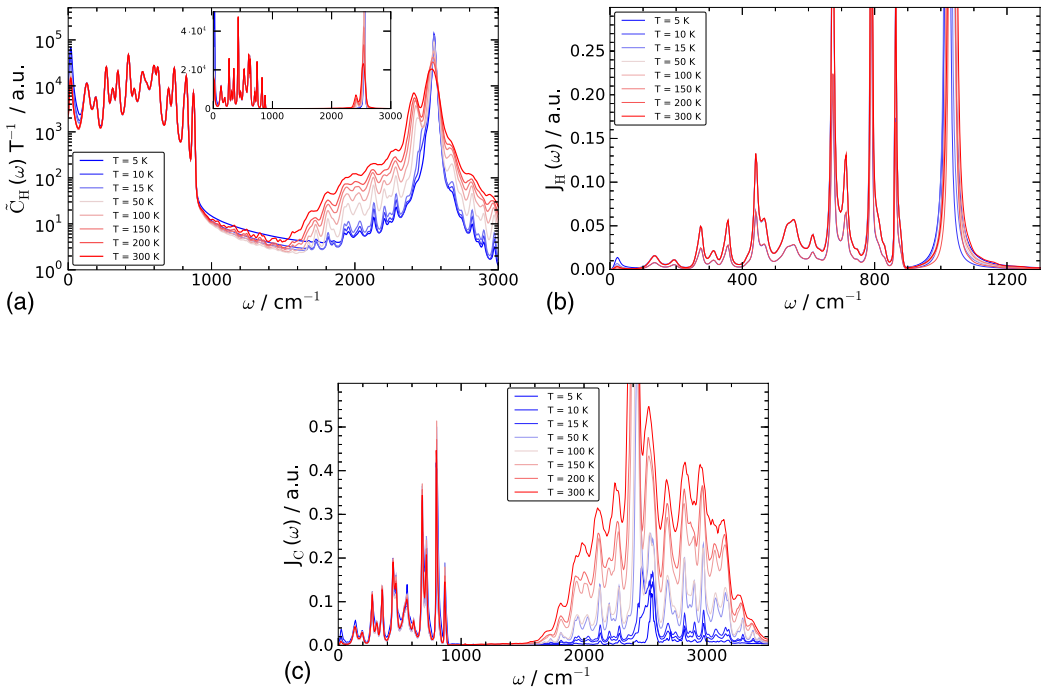

FIG. 3. Spectral functions obtained from molecular dynamics simulations with the source potential model described in the main text. From (a) to (c), (i) a semi-log plot of the temperature scaled correlation function $C(\omega)T^{-1}$, (ii) the spectral density of the coupling on the H atom ($J_H(\omega)$), and (iii) the spectral density of the coupling on the C atom ($J_C(\omega)$). The different curves correspond to different values of the temperature in the range 5-300 K, color coded from blue to red for increasing values of T. Spectral function are given in atomic units and the inset in panel (a) is a linear plot of the same graph.

Application of Eq. (5) gives the spectral density acting on the hydrogen atom, $J_H(\omega)$. This function is negligible above ~1200 cm^{-1}, where a remnant of the high-frequency stretching peak in $\tilde{C}_H(\omega)$ appears but it is orders of magnitude smaller than the values shown in Fig. 3 (panel (b)). As depicted in that figure, the SD contains a broad 0-900 cm^{-1} band, describing the (strong) coupling of the C–H surface stretching mode with the rest of the lattice, and a peak at ~1100 cm^{-1} in correspondence with the bending mode. The latter is slightly temperature dependent, more likely as a consequence of the same anharmonicity reason described above (notice that we are probing the motion of the hydrogen atom coordinate z_H, which contains both surface stretching, bending, and stretching contributions).

Further application of the Cauchy transform through Eq. (6) gives the spectral density on the carbon atom $J_C(\omega)$ which forms the basis of the IO model of Eq. (3). As shown in Fig. 3 (panel (c)), and similarly to $\tilde{C}_H(\omega)$, $J_C(\omega)$ presents a clear separation between the region of the low frequency surface mode and that of the high frequency stretching mode. The low frequency region is again rather stable with temperature and describes the interaction of the C–H unit with the lattice phonon bath. This was confirmed with an independent check where we performed a direct analysis of the source potential and of the coupling it gives rise to. In this case, the spectral density on the carbon atom $J_C(\omega)$ was obtained by the small-amplitude expansion around the equilibrium structure through the expression

$$J_C(\omega) \approx \frac{\pi}{2} \sum_k \frac{c_k^2}{\Omega_k} \Delta(\omega - \Omega_k), \tag{9}$$

where k runs over "constrained" normal modes of the carbon cluster $\tilde{Q}_k$, Ω_k are the corresponding eigenfrequencies, $\Delta(x)$ is a broadened δ–peak, and the coupling coefficients c_k are given by

$$c_k = \frac{\partial^2 V_{at}}{\partial z_C \partial \tilde{Q}_k}(\mathbf{x}_H, z_C, \mathbf{Q})\Big|_{\text{eq}},$$

where $\mathbf{Q} = \mathbf{Q}(\tilde{Q}_1, \ldots, \tilde{Q}_N)$. Here, the constrained modes $\tilde{Q}_k$ were defined to be the normal modes of the lattice when the system coordinates were held fixed at the global equilibrium position. As illustrated in Fig. 4, the resulting $J_C(\omega)$ compares reasonably well with the SDs shown in the panel (c) of Fig. 3, the slight discrepancy being likely a boundary effect only. Indeed, while the potential-based approach used the finite cluster model, the trajectory-based approach employed Langevin atoms at the cluster edge to mimic the infinite lattice, thereby effectively coupling (renormalizing) the long wavelength (low frequency) modes with a continuum. Of course, since none of the constrained eigenfrequencies exceeded the lattice cut-off frequency, $J_C(\omega)$ obtained in this way has a strict Debye cutoff, $\omega_D \sim 900$ cm^{-1}.

To understand the origin of the structure of $J_C(\omega)$ at high frequencies, additional MD simulations were performed with a modified potential,

$$\begin{aligned} V_{at}(\boldsymbol{x}_H, z_C, \boldsymbol{Q}) \\ \rightarrow V_{at}(\boldsymbol{x}_H, z_C, \boldsymbol{Q}) - V_{CH}(\mathbf{x}_H^{\parallel}, z_H - Q_0, z_C - Q_0) \\ + V_{CH}^{(2)}(\mathbf{x}_H^{\parallel}, z_H - Q_0, z_C - Q_0) \end{aligned} \tag{10}$$

in which the 4D potential of the system V_{CH} was replaced by its quadratic expansion $V_{CH}^{(2)}$ around the global minimum. The resulting carbon atom SDs for the harmonic C–H system, as obtained at two different temperatures, are depicted in Fig. 5 where it is evident that the major source of broadening in the high-frequency region is the *anharmonicity* of the system potential. As mentioned above, this can be considered a remediable failure of one of our assumptions of Section II, since the IO model of Eq. (3) correctly includes the full (anharmonic) C–H potential. We ruled out other possible failures by performing additional tests with C–H constrained in the collinear configuration: the results of such calculations, reported in Fig. 6, show that energy transfer effectively occurs *only* through the heights of the C and H atoms, at least with our model potential. Thus, the residual peak and the accompanying background which persist despite the linearization of the model are either a signature of non-linearities in the system-environment coupling or, more likely, just artifacts of the MD.

In general, though, any partial failure of our assumptions (e.g., the above mentioned sequential energy transfer) is necessarily mapped into a fictitious relaxation pathway, thereby contributing to the broadening of the high-frequency peak. For instance, it may well be that bending-mediated relaxation

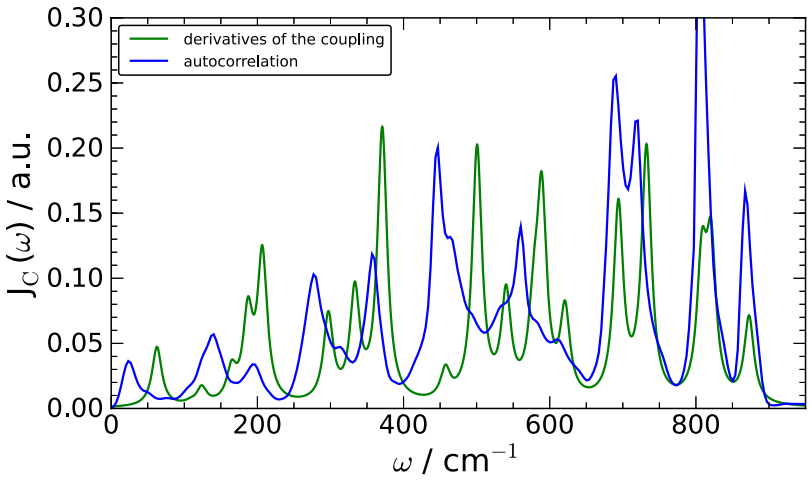

FIG. 4. The spectral density of the coupling on the carbon atom $J_C(\omega)$ as computed from the analysis of the source potential (green line, see text for detail). Also shown for comparison, the trajectory-based spectral density reported in panel (c) of Fig. 3 (blue line, T = 5 K).

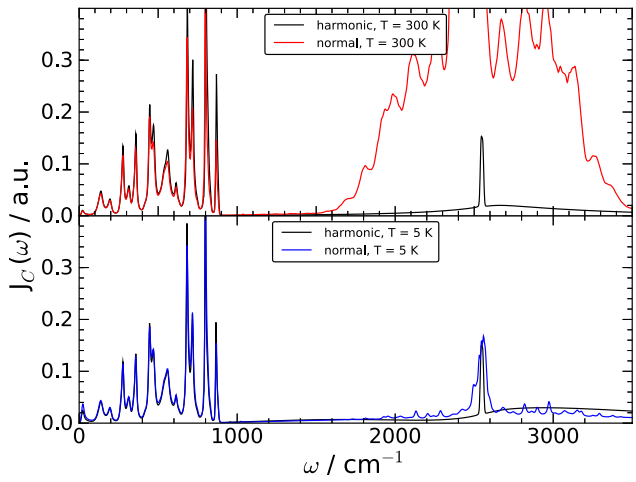

FIG. 5. Harmonic approximation to the source model potential. The figure shows a comparison between the spectral density of the coupling on the carbon atom $J_C(\omega)$ obtained with the original potential (colored curves) and its harmonic approximation (black), both at low and at a high temperature (top and bottom panel for 5 K and 300 K, respectively).

becomes an operative energy relaxation pathway when relaxing the rotationally invariant approximation on the C–H interaction but, according to the protocol outlined in Section II, it will be necessarily mapped into a high-frequency "bath." Determining whether these contributions have a true "physical" origin (and can thus be used as a surrogate of more complicated interactions which cannot be captured by the IO Hamiltonian coupling model) is generally a hard task. For instance, in the example above of a bending-mediated relaxation, only part of the bending-stretching coupling would fall into the system potential (hence generate "spurious" contributions to $J_C(\omega)$) since the in-plane motion of the C atom and its coupling with the lattice are not included in our modeling and their contribution should be better considered as "physical." Fortunately, in this work, we are mainly interested in the sticking dynamics and for this process the high frequency region of $J_C(\omega)$ is irrelevant (see Paper II). A simple extension of the IO model with an exponential coupling based on the properties of the "true"

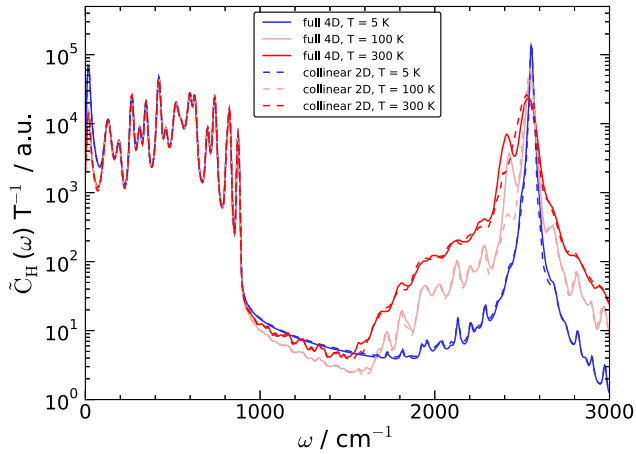

FIG. 6. The temperature scaled auto-correlation $\tilde{C}_H(\omega)\,T^{-1}$ as computed with either the original 4D system potential (solid lines) or its restriction to the 2D collinear arrangement (dashed lines), at three different temperatures $T = 5$ K, 100 K, and 300 K.

bath only (i.e., on the SD at frequencies smaller than ω_D) has been discussed in Ref. 40. It only requires an additional length scale α^{-1} for the interaction that can be obtained, at least in principle from the knowledge of the full potential once the transformation to effective modes[41–44,55] has been performed, namely, through

$$\alpha = -\frac{1}{3\bar{D}_0}\frac{\partial^3 V_{at}}{\partial^2 \bar{X}_1 \partial z_C}$$

where $\bar{X}_1$ is the first effective mode and $\bar{D}_0$ its coupling strength to z_C. Such exponential coupling model seems to be most appropriate in typical situations where vibrational relaxation occurs, i.e., as a consequence of a close contact between the vibrator and its environment.

In closing this section, we show that $J_C(\omega)$ computed at the lowest temperature considered ($T = 5$ K) is consistent with the correlation functions $\tilde{C}_H(\omega)$ we started from, *irrespective* of the temperature. To this end, we set up a classical IO Hamiltonian of Eq. (3) and performed molecular dynamics simulations to compute $C_H^{IO}(\omega)$ (see Table III for details). We employed 300 bath oscillators, evenly arranged in frequency up to 1000 cm^{-1} in order to include only the low frequency region. The results of these test calculations are reported in Fig. 7 and show a remarkable agreement with respect to the position of the peaks, with only minor differences in the heights of the low-frequency peaks which are very sensitive to the long time behavior of the dynamics and, thus, to the discretization of the bath and the time truncation. The agreement is very good in the low frequency region of the spectrum but remarkable in the high frequency region, too. This strongly supports the idea that the broadening of the 2500 cm^{-1} peak mainly comes from the anharmonic shape of the system potential, which is transferred unaltered in the IO model. Additionally, these results clearly show that the harmonic bath of the IO model is well suited to capture all the relevant properties of the stochastic force exerted by the graphene lattice, at least in the low energy regime which is most relevant for our purposes.

B. Vibrational relaxation

As a first quantum test of our IO model, we studied the vibrational relaxation dynamics of the C–H bond following the evolution of an initial state where the system was prepared in an eigenstate of the 4D potential and allowed to relax because of the interaction with the bath (initially in its

TABLE III. Parameters of the MD simulations using the derived IO model.

Number of trajectories	1000
Bath cut-off frequency ω_D	1000 cm^{-1}
Number of oscillators F	300
Mass of the oscillators μ	12.0 amu
Temperature	5, 100, 300 K
Equilibration Δt	0.02 fs
Equilibration $\tau_{relax} = \gamma^{-1}$	5.0 fs
Equilibration time	2.0 ps
Time step Δt	0.01 fs
Propagation time	10.0 ps

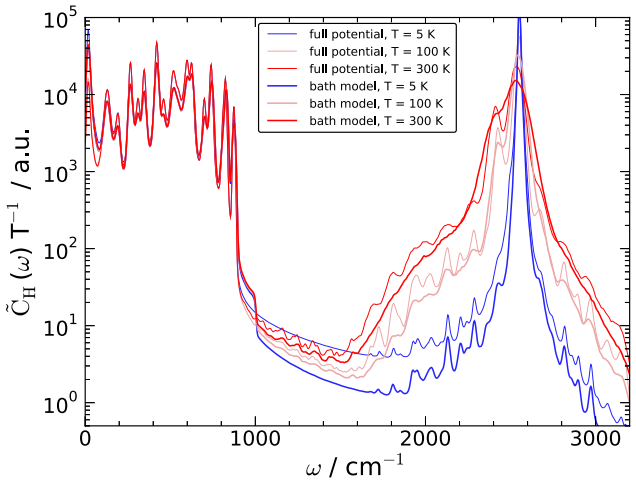

FIG. 7. Temperature scaled position autocorrelation function of the hydrogen atom $C_H(\omega)\,T^{-1}$ as computed with the lattice model (thin lines) and the derived IO model (thick line), at three different temperatures $T = 5$ K, 100 K, and 300 K. The IO model used the $T = 5$ K spectral density $J_C(\omega)$ shown in Fig. 3, truncated at $\omega_D = 1000$ cm^{-1}.

ground-state, to mimic a $T = 0$ K situation). This can be considered a preliminary study of the sticking problem that is addressed in Paper II and that represents the limiting case where the initial "vibrational" eigenstate of the system is picked up from the continuum. Vibrational eigenstates of the 4D potential were obtained by exact (Lanczos) diagonalization, as implemented in the Heidelberg's MCTDH package. Computed eigenvalues are collected in Table IV, labeled by the relevant quantum numbers: $\nu_{\mathrm{s,CH}}$ for the C–H stretching, $\nu_{\mathrm{s,surf}}$ for the surface stretching, and ν_{b} for the C–H bending. Stretching and bending quantum numbers were assigned by comparison with the expected harmonic spectrum, after taking into account the strong anharmonicity of the C–H stretching. The anharmonicity is evident already from the position of the $\nu_{\mathrm{s,CH}} = 1$ state that has an excitation energy of only 2257 cm^{-1}, i.e., much lower than the value of the frequency we found at the bottom of the potential well (2549 cm^{-1}).

Similar to the classical IO case considered above, the independent oscillator Hamiltonian employed for the quantum simulations used the spectral density $J_C(\omega)$ computed at 5 K

TABLE IV. Low energy bound states of the 4D full potential of the C–H system. Values in parentheses refer to the potential constrained to the collinear configuration (2D).

	E / cm^{-1}	$\nu_{\mathrm{s,surf}}$	$\nu_{\mathrm{s,CH}}$	ν_{b}
0	0.00	0	0	0
1	460.87 (468.95)	1	0	0
2	920.11 (937.75)	2	0	0
3	1183.26	0	0	1
4	1378.14 (1406.37)	3	0	0
5	1638.82	1	0	1
6	1835.29 (1874.77)	4	0	0
7	2091.24	2	0	1
8	2199.00 (2257.39)	0	1	0
9	2291.86 (2342.95)	5	0	0
10	2371.74	0	0	2

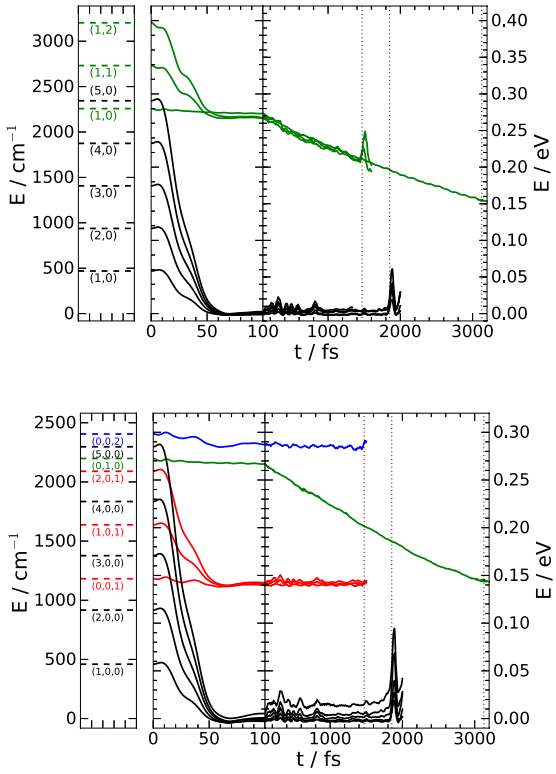

FIG. 8. Vibrational relaxation of the C–H excited state. Time evolution of the system energy (as defined in the text) from different initial vibrational states, for the 2D collinear case (top panel) and for the full 4D case (bottom panel). Panels on left give the vibrational energy spectrum of the system and quantum labels for the 2D ($(\nu_{s,surf}, \nu_{s,CH})$) and the 4D ($(\nu_{s,surf}, \nu_{s,CH}, \nu_b)$) cases (top and bottom panels, respectively). The dashed lines mark the recurrence time t_{rec} of the bath models adopted ($t_{rec} = 1853$, 3127, and 1471 fs for model baths I, II, and III, respectively, see text for details).

in order to minimize the appearance of anharmonic effects of the system in the bath. In contrast with the molecular dynamics simulations, though, we also made use of the high frequency region of $J_C(\omega)$ and thus included in our modeling a relaxation mechanism for the C–H stretching that would be otherwise absent (at least with the model potential adopted in this work). Thus, simulations of the relaxation dynamics of the stretching mode are just representative of what one can expect when a similar $J_C(\omega)$ is used as a surrogate of a more complicated system-environment coupling. Even though this relaxation incidentally turns out to occur on the right time scale, the coupling encoded in $J_C(\omega)$ at these frequencies has little physical meaning and more than likely reflects artifacts of the MD approach (for a thorough investigation on this point, we refer to Ref. 40).

Quantum dynamical calculations were performed using the MCTDH method, as described in Section IV, using three different bath discretization schemes: a low frequency model suited for relaxation of low-frequency modes (model I, with $\omega \in [0, 900]$ cm^{-1}), a high-frequency one optimized for the relaxation of the stretching mode (model II, $\omega \in [2100, 2900]$ cm^{-1}), and a combination of both (model III) to investigate combined excitation of different modes. Different frequency spacings were adopted in each case, and the resulting recurrence times t_{rec} turned out be 1853, 3127, and 1471 fs, respectively. Fig. 8 shows the time evolution of

the system energy in the 2D collinear and full 4D cases, for the first excited states of the system potential. This energy is defined as the expectation value of the system Hamiltonian *plus* half the value of the interaction energy in order to account for the energy that at any time is in the coupling term; the adopted splitting of the total energy can be justified with the help of the virial theorem.[56] As illustrated in Fig. 8, relaxation from the surface stretching proceeds over a very short time scale and is complete in a few tens of fs. On such a small time scale excitation of the bath involves a rather large range of frequencies around the resonant one ($\omega \approx 460$ cm^{-1}), as illustrated in Fig. 9 (top panel), which shows the average occupation number of the bath oscillators during the $\nu_{s,surf} = 1$ relaxation dynamics. Notwithstanding the fast relaxation dynamics, the energy decays reported in Fig. 8 show essentially a Markovian behavior, except for the slippage at short times which extends for a considerable fraction of the relaxation window. This feature is related to the prepared initial states and to the switching on of the coupling term, which actually causes a slight *increase* of the system energy. The opposite behavior is seen in the relaxation of the C–H stretching mode that takes place over a picosecond scale and seems to be complete on a time scale much larger than the 3.0 ps limit imposed by the recurrence time of our bath discretization. In this weak coupling limit, energy is exchanged with quasi-resonant bath oscillators only, as is evident from Fig. 9 (bottom panel) which shows the average occupation number for the stretching mode relaxation. Notice that the quasi-resonant frequencies do not correspond to the spurious 2550 cm^{-1} peak of the $J_C(\omega)$ spectral density since the first excited state of the C–H stretching mode has a considerably lower excitation frequency (2257 cm^{-1}) because of the strong anharmonicity of the system potential. Hence, the resulting relaxation rate ($\tau \sim 5.0$ ps) is determined by the background only, whose origin is not as clear as that of the main peak. Its magnitude is incidentally close to the result obtained by Sakong and Kratzer,[48] who applied perturbation theory from *first principles* and found $\tau = 5.2$ ps.

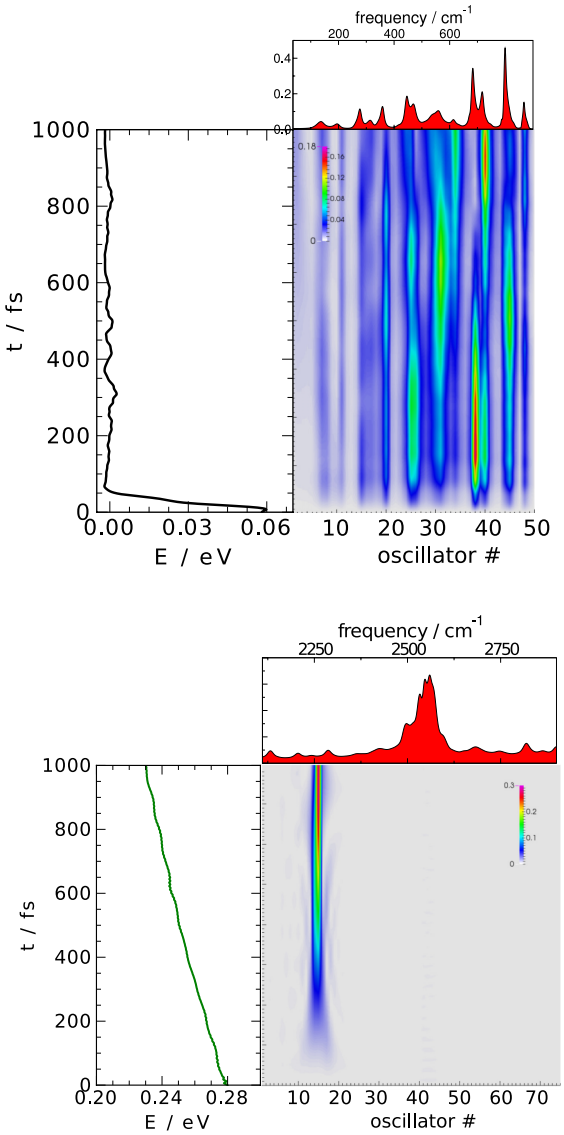

FIG. 9. Time evolution of the average excitation number of the bath oscillators during relaxation of the $\nu_{s,surf} = 1$ state (top panel) and the $\nu_{s,CH} = 1$ state (bottom panel) of the system potential. Along with the bath excitation, the energy of the system is shown.

Finally, we further compared the full dynamical model with the reduced-dimensional 2D collinear one in the relaxation dynamics and found that relaxation of the stretching modes is hardly affected by the inclusion of the additional coordinates (compare top and bottom of Fig. 8). This finding agrees well with the features of our system potential, namely, the lack of coupling between ρ and the heights of the C and H atoms above the surface, for configurations close to linearity.

VI. CONCLUSIONS

We have presented a system bath model that captures the essential physics of a hydrogen atom chemisorbed on graphene and is ideally suited for high-dimensional wavepacket investigations of its quantum dynamics. The system comprises the hydrogen atom and the height of the carbon atom involved in bonding and is described by a 4D potential energy surface based on density functional theory data. The interaction with the rest of the lattice, as subsumed in the spectral density of the environmental couplings felt by the carbon atom, has been obtained by inverting classical information about the hydrogen atom dynamics, with the help of a "source" potential previously developed by one of the present authors. The proposed approach though is rather general and easily accommodates improvements in the system potential and/or in the HC-lattice coupling, and work is already in progress to apply *ab initio* molecular dynamics for obtaining a Hamiltonian model from *first principles* only. The inversion procedure which led us to the working system-bath model has been described in detail and thoroughly checked. As an example of application to dynamical problems, the resulting independent oscillator model has been used to investigate the quantum dynamics of vibrational relaxation at $T = 0$ K with the help of the multi-configuration time-dependent Hartree method. A related paper extends this study to the sticking dynamics.[57]

ACKNOWLEDGMENTS

This work has been supported by Regione Lombardia and the CINECA High Performance Computing Center through a LISA Initiative (2014) grant. B. Jackson gratefully acknowledges support from the Division of Chemical Sciences, Office of Basic Energy Science, Office of Energy Research, U.S. Department of Energy, under Grant No. DE-FG02-87ER13744.

[1]D. C. Elias, R. R. Nair, T. M. G. Mohiuddin, S. V. Morozov, P. Blake, M. P. Halsall, A. C. Ferrari, D. W. Boukhvalov, M. I. Katsnelson, A. K. Geim, and K. S. Novoselov, Science **323**, 610 (2009).
[2]R. Balog, B. Jorgensen, L. Nilsson, M. Andersen, E. Rienks, M. Bianchi, M. Fanetti, E. Laegsgaard, A. Baraldi, S. Lizzit, Z. Sljivancanin, F. Besenbacher, B. Hammer, T. G. Pedersen, P. Hofmann, and L. Hornekaer, Nat. Mater. **9**, 315 (2010).
[3]R. J. Gould and E. E. Salpeter, Astrophys. J. **138**, 393 (1963).
[4]D. Hollenbach and E. E. Salpeter, Astrophys. J. **163**, 155 (1971).
[5]S. T. Bromley, T. P. M. Goumans, E. Herbst, A. P. Jones, and B. Slater, Phys. Chem. Chem. Phys. **16**, 18623 (2014).
[6]L. Jeloaica and V. Sidis, Chem. Phys. Lett. **300**, 157 (1999).
[7]X. Sha and B. Jackson, Surf. Sci. **496**, 318 (2002).
[8]N. Rougeau, D. Teillet-Billy, and V. Sidis, Chem. Phys. Lett. **431**, 135 (2006).
[9]S. Casolo, O. M. Lovvik, R. Martinazzo, and G. F. Tantardini, J. Chem. Phys. **130**, 054704 (2009).
[10]Y. Ferro, S. Morisset, and A. Allouche, Chem. Phys. Lett. **478**, 42 (2009).
[11]M. Bonfanti, R. Martinazzo, G. F. Tantardini, and A. Ponti, J. Phys. Chem. C **111**, 5825 (2007).
[12]J. Ma, A. Michaelides, and D. Alfè, J. Chem. Phys. **134**, 134701 (2011).
[13]M. Bonfanti, S. Casolo, G. F. Tantardini, A. Ponti, and R. Martinazzo, J. Chem. Phys. **135**, 164701 (2011).
[14]Y. Wang, H.-J. Qian, K. Morokuma, and S. Irle, J. Phys. Chem. A **116**, 7154 (2012).
[15]L. Hornekær, E. Rauls, W. Xu, Ž. Šljivančanin, R. Otero, I. Stensgaard, E. Lægsgaard, B. Hammer, and F. Besenbacher, Phys. Rev. Lett. **97**, 186102 (2006).
[16]A. Allouche and Y. Ferro, Phys. Rev. B **74**, 235426 (2006).
[17]D. W. Boukhvalov, M. I. Katsnelson, and A. I. Lichtenstein, Phys. Rev. B **77**, 035427 (2008).
[18]M. Casartelli, S. Casolo, G. F. Tantardini, and R. Martinazzo, Carbon **77**, 165 (2014).
[19]X. Sha and B. Jackson, J. Am. Chem. Soc. **126**, 13095 (2004).
[20]Z. Medina and B. Jackson, J. Chem. Phys. **128**, 114704 (2008).
[21]B. Lepetit, D. Lemoine, Z. Medina, and B. Jackson, J. Chem. Phys. **134**, 114705 (2011).
[22]B. Lepetit and B. Jackson, Phys. Rev. Lett. **107**, 236102 (2011).
[23]E. R. M. Davidson, J. Klimeš, D. Alfè, and A. Michaelides, ACS Nano **8**, 9905 (2014).
[24]L. Hornekær, W. Xu, R. Otero, E. Lægsgaard, and F. Besenbacher, Chem. Phys. Lett. **446**, 237 (2007).
[25]R. Balog, B. Jørgensen, J. Wells, E. Lægsgaard, P. Hofmann, F. Besenbacher, and L. Hornekær, J. Am. Chem. Soc. **131**, 8744 (2009).
[26]J. Kerwin and B. Jackson, J. Chem. Phys. **128**, 084702 (2008).
[27]X. Sha, B. Jackson, D. Lemoine, and B. Lepetit, J. Chem. Phys. **122**, 014709 (2005).
[28]J. Kerwin, X. Sha, and B. Jackson, J. Phys. Chem. B **110**, 18811 (2006).
[29]S. Morisset, Y. Ferro, and A. Allouche, J. Chem. Phys. **133**, 044508 (2010).
[30]S. Cazaux, S. Morisset, M. Spaans, and A. Allouche, Astron. Astrophys. **535**, A27 (2011).
[31]S. Garashchuk, J. Jakowski, L. Wang, and B. G. Sumpter, J. Chem. Theory Comput. **9**, 5221 (2013).
[32]F. Karlický, B. Lepetit, and D. Lemoine, J. Chem. Phys. **140**, 124702 (2014).
[33]T. Aizawa, R. Souda, S. Otani, Y. Ishizawa, and C. Oshima, Phys. Rev. B **42**, 11469 (1990).
[34]M. Dion, H. Rydberg, E. Schröder, D. C. Langreth, and B. I. Lundqvist, Phys. Rev. Lett. **92**, 246401 (2004).
[35]J. Klimes and A. Michaelides, J. Chem. Phys. **137**, 120901 (2012).
[36]U. Weiss, *Quantum Dissipative Systems*, 3rd ed. (World Scientific, Singapore, 2008).
[37]The shift z_C^{eq} is not essential and can be removed with a transformation of the bath coordinates $x_k \to x'_k = x_k + c_k/\omega_k^2 z_C^{eq}$. Friction on the carbon atom is state-independent, *i.e.*, it is the same irrespective of the value of z_C.
[38]R. Kubo, M. Toda, and N. Hashitsume, *Statistical Physics II—Nonequilibrium Statistical Mechanics*, Springer Series in Solid-State Sciences Vol. 31, 2nd ed. (Springer Verlag, 1991).
[39]Equivalently, one can use the velocity autocorrelation function $\ddot{C}_H(t) = -\frac{d^2}{dt^2}C_H(t)$.
[40]M. Bonfanti, K. H. Hughes, I. Burghardt, and R. Martinazzo, "Vibrational relaxation and decoherence in structured environments: A numerical investigation," Ann. Phys. (published online 2015).
[41]K. H. Hughes, C. D. Christ, and I. Burghardt, J. Chem. Phys. **131**, 024109 (2009).
[42]K. H. Hughes, C. D. Christ, and I. Burghardt, J. Chem. Phys. **131**, 124108 (2009).
[43]R. Martinazzo, B. Vacchini, K. H. Hughes, and I. Burghardt, J. Chem. Phys. **134**, 011101 (2011).
[44]R. Martinazzo, K. H. Hughes, and I. Burghardt, Phys. Rev. E **84**, 030102(R) (2011).
[45]A. Luntz and J. Harris, Surf. Sci. **258**, 397 (1991).
[46]Notice though that the model is of *cluster* type and thus cannot account for long wavelength modes.
[47]E. Ghio, L. Mattera, C. Salvo, F. Tommasini, and U. Valbusa, J. Chem. Phys. **73**, 556 (1980).
[48]S. Sakong and P. Kratzer, J. Chem. Phys. **133**, 054505 (2010).
[49]E. Vanden-Eijnden and G. Ciccotti, Chem. Phys. Lett. **429**, 310 (2006).
[50]The cut-off value ω_0 was chosen to be larger than the CH stretching frequency but small enough to smoothly damp the growing baseline at high frequencies.
[51]G. A. Worth, M. H. Beck, A. Jäckle, and H.-D. Meyer, The MCTDH Package, Version 8.2, (2000). H.-D. Meyer, Version 8.3 (2002), Version 8.4 (2007), Version 8.5 (2011). Current version: 8.5.3 (2013). See http://mctdh.uni-hd.de.
[52]H.-D. Meyer, U. Manthe, and L. S. Cederbaum, Chem. Phys. Lett. **165**, 73 (1990).
[53]M. H. Beck, A. Jäckle, G. A. Worth, and H.-D. Meyer, Phys. Rep. **324**, 1 (2000).
[54]*Multidimensional Quantum Dynamics: MCTDH Theory and Applications*, edited by H.-D. Meyer, F. Gatti, and G. A. Worth (Wiley-VCH, Weinheim, 2009).
[55]Differently from the cited references, the modes have been given a (irrelevant) mass and have thus units of length, see also Appendix A in Ref. 40.
[56]M. Nest and H.-D. Meyer, J. Chem. Phys. **119**, 24 (2003).
[57]M. Bonfanti, B. Jackson, K. H. Hughes, I. Burghardt, and R. Martinazzo, "Quantum dynamics of hydrogen atoms on graphene. II. Sticking," J. Chem. Phys. **143**, 124704 (2015).